Inorganic Chemistry
Article

Inorg. Chem. **2010**, *49*, 11325–11332 **11325**
DOI: 10.1021/ic101089n

One Pot Synthesis of Heterometallic 3d−3d Azide Coordination Architectures: Effect of the Single-Ion Anisotropy

Jiong-Peng Zhao,[†] Bo-Wen Hu,[†] Xiao-Feng Zhang,[†] Qian Yang,[†] M. S. El Fallah,[‡] J. Ribas,[‡] and Xian-He Bu*[,†]

[†]*Department of Chemistry, Nankai University, Tianjin 300071, People's Republic of China, and*
[‡]*Departament de Química Inorgànica, Universitat de Barcelona, Diagonal, 647, 08028-Barcelona, Spain*

Received May 30, 2010

Five new isomorphic three-dimensional (3D) heterometallic 3d−3d azide complexes, $[CuNi_{1-x}Co_x(N_3)_2(isonic)_2]_\infty$ ($x = 0$ for **1**, $x = 0.3$ for **2**, $x = 0.5$ for **3**, $x = 0.6$ for **4**, and $x = 1$ for **5**), were obtained by assembling Cu^{II}, M^{II} (Ni^{II} and Co^{II}), azide, and pyridyl carboxylate in hydrothermal condition. The 3D structure can be described as end on (EO) azide and *syn,syn* carboxylates mixed bridged alternate Cu−M chains linked by the pyridyl groups. Dominant ferromagnetic interactions were observed between the Cu^{II} and M^{II} ions in the chains. At low temperature diverse magnetic phenomena were presented in those complexes. As the Ni^{II} ions were replaced by Co^{II} ions with large anisotropy, the magnetism of the complexes change gradually from metamagnet to single-chain magnet (SCM)-like behaviors.

Introduction

Design and synthesis of molecule based nanomagnets has become one of the most active fields in molecular magnetism because of their unusual physical properties and their potential importance for high-density data storage and quantum-computing applications.[1,2] As such molecule magnets, single-molecule magnets (SMMs), were widely investigated, since the first SMMs were discovered in 1993.[3] However, during the past few years, this branch of molecular magnetism dealing with one-dimensional (1D) magnet so-called single-chain magnets (SCMs) has become an area of intense research activity since they might afford extended correlation lengths of the magnetization at comparatively higher temperatures by comparing with SMMs.[4] In order to realize the SCMs, some key points must be taken into account: strong uniaxial Ising-type anisotropy; ferro-, ferrimagnetic or weak ferromagnetic state; and high ratio between intra- (J) and interchain (J') magnetic interactions.[4,5] Recently, some 3D entities showed interesting SCM-like behaviors for much weaker interchain interactions conducted by the long ligands between 1D chains compared to intrachain.[6] That provides a new way to construct SCM-like complexes.

As a versatile bridging ligand with various exchange pathways, the azide ligand is a good candidate for the design of molecule magnets. In this sense, several 1−3D complexes have been reported as well as a few nanomagnets.[7] Due to the explosive character of azide compounds and no appropriate metal-azide building blocks for "metal complex as ligand", the study of magnetism in the field of heterometallic 3d−3d azide complex is still rare,[8] and the study of magnetism in the field of high-dimensional heterometallic 3d−3d azide complexes is still a virgin soil. It is interesting to introduce two kinds of metal ions in the metal−azide systems, which will

*Corresponding author. E-mail: buxh@nankai.edu.cn. Telephone: +86-22-23502809.

(1) For examples: (a) Thomas, L.; Lionti, F.; Ballou, R.; Gatteschi, D.; Sessoli, R.; Barbara, B. *Nature* **1996**, *383*, 145. (b) Friedman, J. R.; Sarachik, M. P.; Tejada, J.; Ziolo, R. *Phys. Rev. Lett.* **1996**, *76*, 3830. (c) Gatteschi, D.; Sessoli, R.; Villain, J. *Molecular Nanomagnets*; Oxford University Press: Oxford, 2006. (d) Gatteschi, D.; Sessoli, R. *Angew. Chem., Int. Ed.* **2003**, *43*, 268. (e) Wernsdorfer, W.; Sessoli, R. *Science* **1999**, *284*, 133.

(2) (a) Caneschi, A.; Gatteschi, D.; Lalioti, N.; Sangregorio, C.; Sessoli, R.; Venturi, G.; Vindigni, A.; Rettori, A.; Pini, M. G.; Novak, M. A. *Angew. Chem., Int. Ed.* **2001**, *40*, 1760. (b) Clérac, R.; Miyasaka, H.; Yamashita, M.; Coulon, C. *J. Am. Chem. Soc.* **2002**, *124*, 12837. (c) Liu, T.-F.; Fu, D.; Gao, S.; Zhang, Y.-Z.; Sun, H.-L.; Su, G.; Liu, Y.-J. *J. Am. Chem. Soc.* **2003**, *125*, 13976. (d) Wang, S.; Zuo, J.-L.; Gao, S.; Zhou, H.-C.; Zhang, Y.-Z.; You, X.-Z. *J. Am. Chem. Soc.* **2004**, *126*, 8900.

(3) (a) Sessoli, R.; Gatteschi, D.; Caneschi, A.; Novak, M. A. *Nature* **1993**, *365*, 141. (b) Coulon, C.; Miyasaka, H.; Clérac, R. *Struct. Bonding* (*Berlin*) **2006**, *122*, 163.

(4) Coronado, E.; Galán-Mascarós, J. R.; Martí-Gastaldo, C. *J. Am. Chem. Soc.* **2008**, *130*, 14987.

(5) (a) Palii, A. V.; Reu, O. S.; Ostrovsky, S. M.; Klokishner, S. I.; Tsukerblat, B. S.; Sun, Z.-M.; Mao, J.-G.; Prosvirin, A. V.; Zhao, H.-H.; Dunbar, K. R. *J. Am. Chem. Soc.* **2008**, *130*, 14729. (b) Glauber, R. J. *J. Math. Phys.* **1963**, *4*, 294.

(6) (a) Zheng, Y.-Z.; Tong, M.-L.; Zhang, W.-X.; Chen, X.-M. *Angew. Chem., Int. Ed.* **2006**, *45*, 6310. (b) Zheng, Y.-Z.; Xue, W.; Tong, M.-L.; Chen, X.-M.; Zheng, S.-L. *Inorg. Chem.* **2008**, *47*, 11202.

(7) (a) Yoon, J. H.; Ryu, D. W.; Kim, H. C.; Yoon, S. W. *Chem.—Eur. J.* **2009**, *15*, 3661. (b) Sun, H.-L.; Wang, Z.-M.; Gao, S. *Chem.—Eur. J.* **2009**, *15*, 1757. (c) Zhang, Y.-Z.; Wernsdorfer, W.; Pan, F.; Wang, Z.-M.; Gao, S. *Chem. Commun.* **2006**, 3302. (d) Zeng, Y. F.; Hu, X.; Liu, F. C.; Bu, X. H. *Chem. Soc. Rev.* **2009**, *38*, 469. (e) Liu, F. C.; Zeng, Y. F.; Jiao, J; Bu, X. H.; Ribas, J.; Batten, S. R. *Inorg. Chem.* **2006**, *45*, 2776. (f) Zeng, Y. F.; Liu, F. C.; Zhao, J. P.; Cai, S.; Bu, X. H.; Riba, J. *Chem. Commun.* **2006**, 2227. (g) Liu, F. C.; Zeng, Y. F.; Zhao, J. P.; Hu, B. W.; Bu, X. H.; Ribas, J.; Cano, J. *Inorg. Chem.* **2007**, *46*, 1520. (h) Zeng, Y. F.; Zhao, J. P.; Hu, B. W.; Hu, X.; Liu, F. C.; Ribas, J.; Ribas-Arino, J.; Bu, X. H. *Chem.—Eur. J.* **2007**, *13*, 9924.

Published on Web 11/16/2010

bring particular structures and properties to heterometallic azide complexes. The magnetic properties of those complexes could be tuned subtly by changing the metal ions with similar coordination geometry.[9] Herein we present three isomorphic azide-bridged heterometallic 3D frameworks $[CuNi_{1-x}Co_x(N_3)_2(isonic)_2]_\infty$ ($x = 0$ for **1**, $x = 0.3$ for **2**, $x = 0.5$ for **3**, $x = 0.6$ for **4**, and $x = 1$ for **5**), obtained from hydrothermal conditions, in which azido ligands bridged Cu^{II} and M^{II} ions giving an alternated chain and an isonicotinate as the coligand supporting the whole network. Interestingly, as the Ni^{II} ions were replaced by Co^{II} ions with large anisotropy, the magnetism of those complexes changes gradually from metamagnet to SCM-like behaviors.

Experimental Section

Materials and Physical Measurements. All the chemicals used for synthesis of the compounds are of analytical grade and commercially available. $CuCl_2 \cdot 2H_2O$, $NiCl_2 \cdot 6H_2O$, $CoCl_2 \cdot 6H_2O$, isonicotinic acid, and sodium azide were purchased from commercial sources and used as received.

Caution*! Azide metal complexes are potentially explosive, only a small amount of material should be prepared with care.*

Elemental analyses (C, H, N) were performed on a Perkin-Elmer 240C analyzer. The metal elements Cu, Ni, and Co were detected by atomic absorption spectrometry (AAS) (Hitachi 180−80). The X-ray powder diffraction (XRPD) was recorded on a Rigaku D/Max-2500 diffractometer at 40 kV and 100 mA for a Cu-target tube and a graphite monochromator. IR spectra were measured on a Tensor 27 OPUS (Bruker) FT-IR spectrometer with KBr pellets. Simulation of the XRPD spectra was carried out by the single-crystal data and the diffraction-crystal module of the mercury (Hg) program available free of charge via the Internet at http://www.iucr.org.

Magnetic data were collected using crushed crystals of the sample on a Quantum Design MPMS-XL SQUID magnetometer equipped with a 5T magnet. The data were corrected using Pascal's constants to calculate the diamagnetic susceptibility; an experimental correction for the sample holder was applied.

Synthesis of 1 and 5. A mixture of $CuCl_2 \cdot 2H_2O$ (0.75 mmol), $MCl_2 \cdot 6H_2O$ (M = Ni (1.5 mol) for **1**, and M = Co (2 mmol) for **5**) and isonicotinic acid (0.75 mmol), NaN_3 (2 mmol) and H_2O (10 mL) was sealed in a Teflon-lined autoclave and heated to 140 °C. After maintained for 48 h, the reaction vessel was cooled to room temperature in 12 h, and the pure primrose black crystals were collected with ca. 20∼25% yield based on $CuCl_2 \cdot 2H_2O$. FT-IR (KBr pellets, cm^{-1}): (**1**) 3415, 3132, 2170, 2084, 2066, 1603, 1555, 1401, 1128, 770, 699, 617; (**5**) 3420, 3132, 2170, 2081, 2063, 1637, 1617, 1401, 1124, 861, 619. Elemental analytical data correspond to: $C_{12}H_8CuN_8NiO_4$ (**1**) Calcd: C%, 31.99; H%,1.79; N%, 24.87%. Found: C, 31.66; H, 1.72; N, 24.79%. $C_{12}H_8CoCuN_8O_4$ (**5**) Calcd: C%, 31.98; H%, 1.79; N%, 24.86%. Found: C, 31.70; H, 1.50; N, 24.52%. AAS (%): (**1**) Cu, 14.40; Ni, 12.99; ratio of Cu:Ni = 1.02:1.00; (**5**) Cu, 14.20; Co, 12.90; ratio of Cu:Co = 1.02:1.

Synthesis of 2−4. The procedures synthesis of the **2**−**4** are similar to that of **1** and **5**. The amounts of $CuCl_2 \cdot 2H_2O$, isonicotinic acid (0.75 mmol), NaN_3 (2 mmol), and H_2O (10 mL) were the same as that of **1** and **5**, however $MCl_2 \cdot 6H_2O$ was replaced by a mixture of $NiCl_2 \cdot 6H_2O$ and $CoCl_2 \cdot 6H_2O$ with a different ratio ($NiCl_2 \cdot 6H_2O$:$CoCl_2 \cdot 6H_2O$ = 1.5 mmol:0.75 mmol for **2**; $NiCl_2 \cdot 6H_2O$: $CoCl_2 \cdot 6H_2O$=2.5 mmol:0.5 mmol for **3**, and $NiCl_2 \cdot 6H_2O$: $CoCl_2 \cdot 6H_2O$ = 0.3 mmol:2 mmol for **4**). The pure primrose black crystals were collected with ca. 20∼25% yield based on $CuCl_2 \cdot 2H_2O$. FT-IR (KBr pellets, cm^{-1}): (**2**) 3418, 2082, 2066, 1587, 1551, 1404, 1286, 1219, 868, 770, 698, 599; (**3**) 3416, 3131, 2170, 2082, 2064, 1612, 1401, 1125, 861, 770, 618; (**4**) 3416, 2083, 2066, 1619, 1601,1551, 1403,1285,1061, 1018, 869, 697, 599. Elemental analytical data correspond to: $C_{12}H_8Co_{0.3}CuN_8Ni_{0.7}O_4$ (**2**) Calcd: C%, 31.99; H%, 1.79; N%, 24.87%. Found: C, 31.62; H, 1.52; N, 24.65%. $C_{12}H_8Co_{0.5}CuN_8Ni_{0.5}O_4$ (**3**) Calcd: C%, 31.98; H%, 1.79; N%, 24.87%. Found: C, 31.58; H, 1.61; N, 25.10%. $C_{12}H_8Co_{0.6}CuN_8Ni_{0.4}O_4$ (**4**) Calcd: C%, 31.98; H%, 1.79; N%, 24.87%. Found: C, 32.12; H, 1.95; N, 24.62%.

In the synthesis, if the amounts of $CuCl_2 \cdot 2H_2O$ used are less than that of $MCl_2 \cdot 6H_2O$ (M = Ni and Co), then it is easy to obtain those complexes $[CuM(N_3)_2(isonic)_2]_\infty$ (M = Ni for **1** and Co for **5**). In the preparation of **5** more $CoCl_2 \cdot 6H_2O$ was used than that of $NiCl_2 \cdot 6H_2O$ in **1** to grow good crystals, that indicates Ni^{II} ions are more reactive than Co^{II} ions. In the synthesis of the intermediates complexes **2**−**4**, the ratio of the Ni:Co are form 1:2−8 in the initial reactants, while it give a results of $[CuNi_{1-x}Co_x(N_3)_2(isonic)_2]_\infty$ ($x \approx 0.3-0.6$) that also confirmed Ni^{II} ions are more reactive than Co^{II} ions. However in the synthesis the complexes **2**−**4**, it is not easy to control the ratios x accurately. From the atomic absorption spectrometry analysis of the products of different pots with the same ratios of the reactants, we found each ratio of the initial reactants can give a result accurate to the first decimal place.

X-ray Data Collection and Structure Determinations. X-ray single-crystal diffraction data for complexes **1**−**5** were collected on a Rigaku SCXmini diffractometer at 293(2) K with Mo Kα radiation ($\lambda = 0.71073$ Å) by ω scan mode. The program SAINT[10a] was used for integration of the diffraction profiles. All the structures were solved by direct methods using the SHELXS program of the SHELXTL package and refined by full-matrix least-squares methods with SHELXL (semiempirical absorption corrections were applied using the SADABS program).[10b] Metal atoms in each complex were located from the *E*-maps, and other non-hydrogen atoms were located in successive difference Fourier syntheses and refined with anisotropic thermal parameters on F^2. The hydrogen atoms of the ligands were generated theoretically onto the specific atoms and refined isotropically with fixed thermal factors. Table 1 shows crystallographic crystal data and structure processing parameters. Selected bond lengths and bond angles are listed in Table 2.

Results and Discussion

Description of Crystal Structure. Single-crystal X-ray diffraction analysis of **1** reveals that the complex crystallize in the monoclinic space group $C2/c$ (see Table 1 for further information about the unit cell) and have a 3D framework structure. The asymmetric unit of **1** contains one unique azide anion, one isonicotinate anion and Cu^{II} and Ni^{II} ions located on special positions. The Cu1 ion located in the inversion center has an elongated octahedral configuration (CuN2O4), resulting from the Jahn−Teller effect (Figure 1a). The apical positions of Cu1 ion are occupied by two symmetrical oxygen atoms from two carboxylate ligands with a bond length of $Cu1-O1^{ii}$/$O1^{vi}$ = 2.585(3) Å. The equatorial plane is formed by two

(8) (a) Colacio, E.; Costes, J.-P.; Domínguez-Vera, J. M.; Maimounac, I. B.; Suaárez-Varela, J. *Chem. Commun.* **2005**, 534. (b) Suaárez-Varela, J.; Maimoun, I. B.; Colacio, E. *Dalton Trans.* **2004**, 3938. (c) Yang, Y.-T.; Luo, F.; Che, Y.-X.; Zheng, J.-M. *Cryst. Growth Des.* **2008**, *8*, 3508. (d) Rajendiran, T. M.; Mathonière, C.; Golhen, S.; Ouahab, L.; Kahn, O. *Inorg. Chem.* **1998**, *37*, 2651.

(9) (a) Zeng, M.-H.; Wang, B.; Wang, X.-Y.; Zhang, W.-X.; Chen, X.-M.; Gao, S. *Inorg. Chem.* **2006**, *45*, 7069. (b) Cooper, G. J. T.; Newton, G. N.; Kögerler, P.; Long, D.-L.; Engelhardt, L.; Luban, M.; Cronin, L. *Angew. Chem., Int. Ed.* **2007**, *46*, 1340. (c) Li, J.-R.; Yu, Q.; Tao, Y.; Bu, X.-H.; Ribas, J.; Batten, S. R. *Chem. Commun.* **2007**, 2290. (d) Li, Z.-X.; Zhao, J.-P.; Carolina, S. E.; Ma, H.; Pan, Z.-D.; Zeng, Y.-F.; Bu, X. H. *Inorg. Chem.* **2009**, *48*, 11601.

(10) (a) Bruker, A. X. S. SAINT Software Reference Manual; Madison, WI, 1998. (b) Sheldrick, G. M. SHELXTL NT Version 5.1. Program for Solution and Refinement of Crystal Structures, University of Göttingen, Germany, 1997.

Table 1. Crystal Data and Structure Refinement for **1**−**5**

	1	**2**	**3**	**4**	**5**
chemical formula	$C_{12}H_8CuNiN_8O_4$	$C_{12}H_8CuCo_{0.3}Ni_{0.7}N_8O_4$	$C_{12}H_8CuCo_{0.5}Ni_{0.5}N_8O_4$	$C_{12}H_8CuCo_{0.6}Ni_{0.4}N_8O_4$	$C_{12}H_8CuCoN_8O_4$
formula weight	450.51	450.58	450.60	450.65	450.73
space group	*C*2/*c*	*C*2/*c*	*C*2/*c*	*C*2/*c*	*C*2/*c*
a (Å)	12.843(3)	12.868(3)	12.848(3)	12.890(3)	12.969(3)
b (Å)	13.229(3)	13.351(3)	13.275(3)	13.350(3)	13.361(3)
c (Å)	10.517(2)	10.526(2)	10.443(2)	10.496(2)	10.446(2)
β (°)	104.44(3)	104.39(3)	104.45(3)	104.45(3)	104.39(3)
V (Å^3)	1730.4(6)	1751.5(6)	1724.7(6)	1749.1(6)	1753.3(6)
Z	4	4	4	4	4
GOF	0.970	1.087	1.155	1.145	1.257
D, g cm^{-3}	1.729	1.709	1.735	1.711	1.708
μ, mm^{-1}	2.353	2.286	2.308	2.251	2.195
T, K	293(2)	293(2)	293(2)	293(2)	293(2)
R^a/wR^b	0.0420/0.0875	0.0644/0.1394	0.0612/0.1031	0.0355/0.0657	0.0590/0.0983

$^a R = \sum||F_o| - |F_c||/\sum|F_o|$. $^b R_w = [\sum[w(F_o^2 - F_c^2)^2]/\sum w(F_o^2)^2]^{1/2}$.

Table 2. Selected bond lengths [°] and angles [Å] for **1**−**5**

	1		
Ni(1)−N(1)	2.096(3)	Cu(1)−O(2)^b	1.960(2)
Ni(1)−O(1)^a	2.098(2)	Cu(1)−N(1)	1.976(3)
Ni(1)−N(4)	2.103(3)	Cu(1)−O(1)^a	2.585(3)
Cu(1)−N(1)−Ni(1)	106.79(13)	Ni(1)^c−O(1)−Cu(1)^d	87.92(8)
	2		
Ni/Co (1)−N(1)	2.076(5)	Cu(1)−O(2)^b	1.954(4)
Ni/Co (1)−O(1)^a	2.108(3)	Cu(1)− N(1)	1.981(4)
Ni/Co(1)−N(4)	2.128(4)	Cu(1)−O(1)^a	2.572(4)
Cu(1)−N(1)−Ni/Co (1)	107.1(2)	Ni/Co(1)^c−O(1)−Cu(1)^d	87.84(13)
	3		
Ni/Co (1)−N(1)	2.106(5)	Cu(1)−O(2)^b	1.962(4)
Ni/Co (1)−O(1)^a	2.113(4)	Cu(1)−N(1)	1.984(5)
Ni/Co(1)−N(4)	2.134(5)	Cu(1)−O(1)^a	2.596(4)
Cu(1)−N(1)−Ni/Co (1)	106.6(2)	Ni/Co(1)^c−O(1)−Cu(1)^d	87.71(14)
	4		
Ni/Co (1)−N(1)	2.099(3)	Cu(1)−O(2)^b	1.962(2)
Ni/Co (1)−O(1)^a	2.120(2)	Cu(1)−N(1)	1.981(3)
Ni/Co(1)−N(4)	2.137(3)	Cu(1)−O(1)^a	2.583(2)
Cu(1)−N(1)−Ni/Co (1)	106.87(12)	Ni/Co(1)^c−O(1)−Cu(1)^d	87.78(8)
	5		
Co(1)−N(1)	2.101(4)	Cu(1)−O(2)^b	1.960(3)
Co(1)−O(1)^a	2.129(3)	Cu(1)−N(1)	1.990(6)
Co(1)−N(4)	2.158(4)	Cu(1)−O(1)#2	2.569(3)
Cu(1)−N(1)−Co(1)	106.59(17)	Co(1)^c−O(1)−Cu(1)^d	87.87(11)

$^a -x + 1/2, y - 1/2, -z - 1/2$. $^b -x + 1/2, -y + 3/2, -z$. $^c x - 1/2, y + 1/2, z$. $^d -x + 1/2, y + 1/2, -z - 1/2$.

oxygen atoms from the carboxylate groups and two nitrogen atoms from azide anions with bond lengths of Cu1−O2^{iii}/O2^{iv} = 1.960(2) and Cu1−N1/N1^{v} = 1.976(3) Å. The Ni1 ion is coordinated by two azide anions, two carboxylate groups, and two pyridyl nitrogen atoms with almost regular octahedron geometry and bond lengths of Ni1−N1/N1^{i} = 2.096(3), Ni1−O1^{ii}/O1^{iii} = 2.098(2), and Ni1−N4/N4^{i} = 2.103(3) Å. It is worth noting that the bond angle of N1−Ni1−N1^{i} is 172.00(15)°, however the angles of N4−Ni1−N4^{i} and O1^{ii}−Ni1−O1^{iii} are 86.06(13)° and 96.86(16)°. The azide anions bridge the Ni1 and Cu1 ions in end on (EO) mode giving a 1D alternating zig chain (Figures 1b and 2d) in which the Cu^{II} ions are in center, but the Ni^{II} ions are in the corner. The Ni1−N1−Cu1 angle is 106.79(13)° and the distance between Ni1 and Cu1 is 3.270 Å. The carboxylate groups link the Ni^{II} ion and two

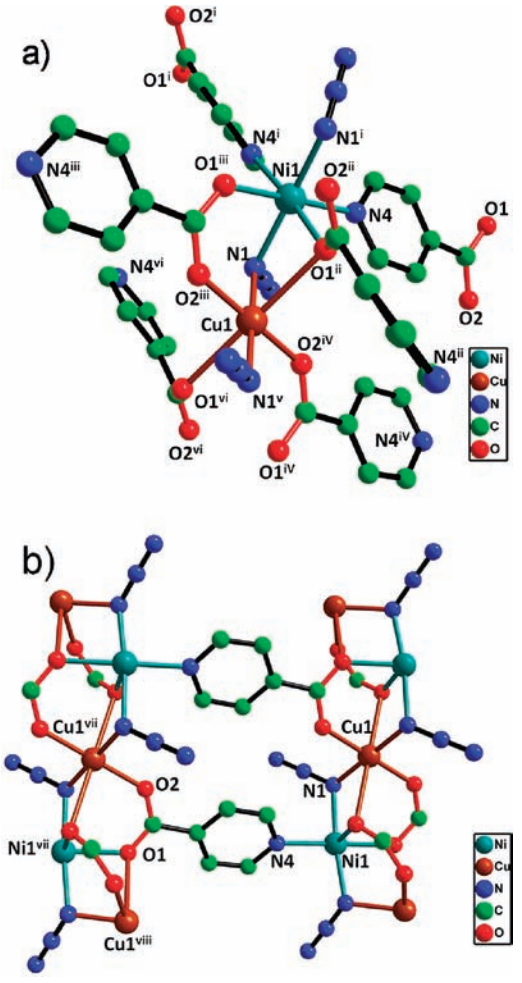

Figure 1. (a) The coordination modes of the metal ions in **1**. (b) The cordination modes of the ligands in **1**. Symmetry codes: (i) $-x + 1, y, -z - 1/2$; (ii) $-x + 1/2, y - 1/2, -z - 1/2$; (iii) $x + 1/2, y - 1/2, z$; (iv) $-x + 1/2, -y + 3/2, -z$; (v) $-x + 1, -y + 1, -z$; (vi) $x + 1/2, -y + 3/2, z + 1/2$; (vii) $x - 1/2, y + 1/2, z$; (viii) $-x + 1/2, y + 1/2, -z - 1/2$.

neighboring Cu^{II} ions in the *syn*, *syn*, *anti*, μ_3-κO:κO′:κO mode in which the O1 bridges two Cu1 ions in apical positions with a bond angle of Ni−O1^{ii}−Cu1 87.92(8)°. The coordination of the carboxylate groups enhances the metal azide chains. The isonicotinate performs a μ_4-bridging mode using the nitrogen and oxygen atoms to link one Ni^{II} and two Cu^{II} ions in one chain and one Ni^{II} ion in

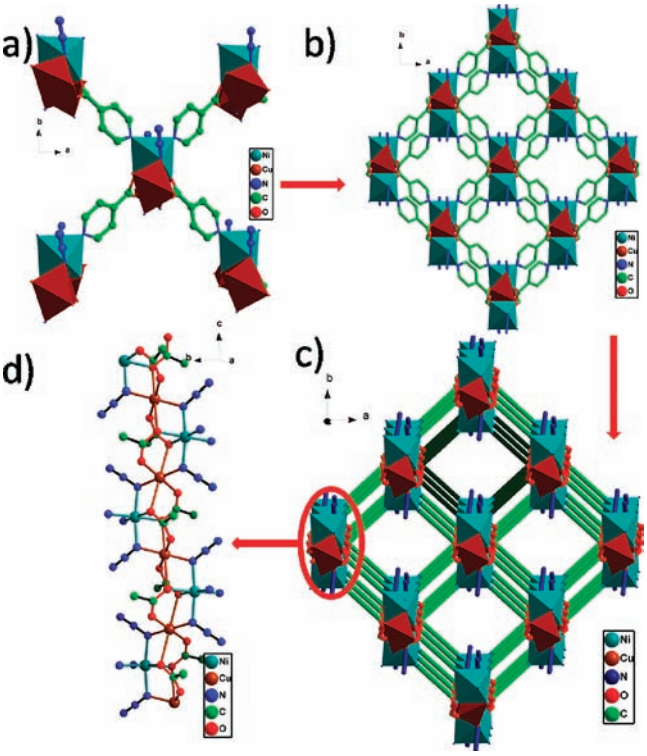

Figure 2. (a) The linkage of the ligands between the chains in **1**. (b) The polyhedron view of the 3D structure of **1**. (c) The simplified 3D view and the double walled channels formed by the isonicotinate ligands (simplified) in **1**. (d) View of the azide carboxylate-mixed coordinating Cu−Ni chain.

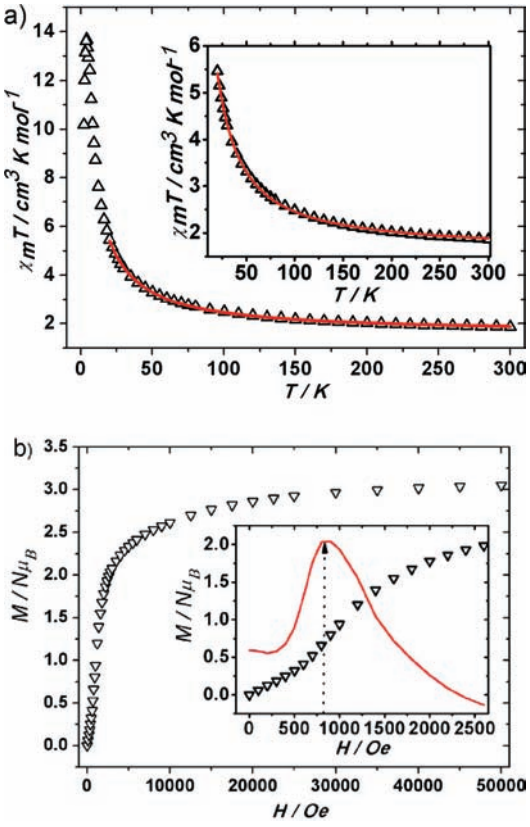

Figure 3. (a) Plots of observed $\chi_m T$ vs T at 0.2 T of **1** (triangles). The solid red line is the best fit to the experimental data. Inset: $\chi_m T$ vs T plot and best fit at 20−300 K of **1**. b) The field-dependent magnetizations plots ($M/N\mu_B$ vs H) plots of **1** at 2 K; Inset: $M/N\mu_B$ vs H plots of **1** at 2 K in the low-field zone (0−2500 Oe), showing the sigmoidal shape of the curve, together with its first derivative (red line). The maximum (800 Oe) corresponds to the critical field of the metamagnetic phase.

the neighbor chain (Figure 1b). The isonicotinate ligands arrange in two different directions alternating between one chain and the neighbors. The 1D chains connect to four adjacent chains forming a 3D open framework (Figure 2), and a 1D channel along the *c* axis was formed (see Figure S1, Supporting Information). It is interesting that the channels have double walls with diagonal distances of 9.7 and 13.2 Å for the inside and outside wells, respectively (Figure 2c).

The complex **2**−**5** are isomorphous with **1**, however the coordination bond lengths of the Ni^{II} and Co^{II} ions reflect on the different metal ions. In **5** the Co^{II}−N/O bond lengths are longer than that of Ni^{II}−N/O in **1**, especially the coordinated bonds involvedin the pyridyl nitrogen atoms (Ni1−N4/N4^i = 2.103(3) Å and Co1−N4/N4^i = 2.158(4) Å). These results slightly compressed the distortion octahedron coordinated geometry of the Co^{II} ions in **5** with the azide ions in the apical positions. The bond details of the Ni^{II}/Co^{II} ions in **2**−**4** are in between that of **1** and **5**, indicating the octahedron-coordinated metal site is located with Ni^{II} and Co^{II} together in complexes **2**−**4**.

Magnetic Studies. Magnetic measurements were carried out on crystalline samples of complexes **1**−**5** (phase purity of samples detected by XRPD; see Figure S2, Supporting Information). As has been discussed above, these compounds are structurally featured as Cu^{II}−M^{II}−N_3/COO chains linked by the isonicotinate ligands. The Cu^{II} ions have an elongated octahedral configuration, and the M^{II} ions have a regular octahedron geometry. From the magnetic point of view, the azide and the carboxylate bridges conduct strong magnetic coupling, while the interactions transferred by the long isonicotinate is weak. Usually, the interactions conducted by azide ions are dependant on the bridging details[11] and the carboxylate-mediated small antiferromagnetic coupling.[12] In these complexes the azide-adopting EO mode bridges Cu^{II} and M^{II} in an equatorial plane with bond angles ca. 107°, so ferromagnetic couplings conducted by azide anions between metal ions would be expected.[11] Actually, a dominant ferromagnetic coupling between Cu^{II}−M^{II} was found in those complex, however at low temperature diverse magnetic phenomena were presented.

The magnetic properties of complex **1** are shown in Figure 3 as $\chi_m T$ vs T and $M/N\mu_B$ vs H, assuming a crystallographic unit CuNi for the molar weight. Starting from room temperature, $\chi_m T$ values smoothly increase up to 50 K and below 50 K increases quickly to a maximum 13.7 cm^3 mol^{-1}K at 4 K before dropping. The values of the best-fit parameters from the magnetic data in the temperature 100−300 K through the Curie−Weiss law (Figure S3, Supporting Information) are θ = 34.68 K and C = 1.67 cm^3 K mol^{-1}; this value is expected for two magnetically isolated spins with S = 1/2 and 1 (g > 2.00) with ferromagnetic interactions. The global features are characteristic of dominant ferromagnetic interactions, with

(11) Ruiz, E.; Cano, J.; Alvarez, S.; Alemany, P. *J. Am. Chem. Soc.* **1998**, *120*, 11122.
(12) Rodríguez-Fortea, A.; Alemany, P.; Alvarez, S.; Ruiz, E. *Chem.—Eur. J.* **2001**, *7*, 627.

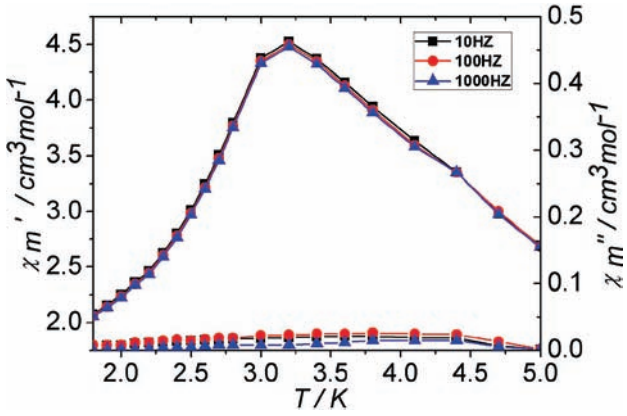

Figure 4. The ac plots for complex **1** between 5 and 2 K.

the presence of the D parameter (Ni^{II} ions) and/or small AF interactions, manifested at low temperatures. The field-dependent magnetizations at 2 K (Figure 3b) clearly corroborate the ferromagnetic coupling. The $M/N\mu_B$ value at 5 T is close to 3.0 $N\mu_B$, which approaches the saturation value for a CuNi pair. However, the curve does not follow the Brillouin function. Indeed, at a very low field, the curve has a weak inflection typical of metamagnetic systems and then rapidly increases almost vertically, suggesting that the ferromagnetic coupling is strong. This metamagnetic behavior can be realized by recording the first derivative of the $M/N\mu_B$ in the 0−2500 Oe (Figure 3b insert). The inflection is clearly seen, and the first derivative shows a clear maximum at ca. 800 Oe. The sigmoidal shape of the magnetization was plotted at very low fields with a value for the critical field (H_c) of ca. 800 Oe, which accounts for a weak antiferromagnetic interaction.

The zero-field-cooled (ZFC) and the field-cooled (FC) curves are completely identical indicating an antiferromagnetic ground state below the critical field (H_c) of ca. 800 G (Figure S4a, Supporting Information). The 3D antiferromagnetic order is confirmed by the ac measurements in an oscillating field 2.5 Oe at different frequencies (Figure 4). Only obvious in-phase χ_m' peaks at 3.2 K are observed, which is consistent with the antiferromagnetic order in **1** below 3.2 K. Furthermore, the small metamagnetic behavior also can be realized by comparing the χ_m curves in low temperature with a different external field. (Figure S4, Supporting Information). It is well-known that $\chi_m = \chi_m' + i\chi_m''$, if $\chi_m'' = 0$, $\chi_m = \chi_m'$. If we compare the χ_m' values (at ca. 0 Oe) with those obtained in a dc measurement (Figure S4b, Supporting Information), then we realize that they are very similar but with the important difference: at ca. 0 Oe there is no possibility of a saturation effect in χ_m values, whereas at 0.2 T the saturation effects avoid the total decreasing of the χ_m values (see Figure S4b, Supporting Information).

As mentioned above the dominating magnetic character of complex **1** is the ferromagnetic spin-alternated $S = 1/2-1$ chains between which are weak antiferromagnetic interactions. This feature gives a spin-alternated $S = 1/2-1$ system (Figure 2d). There are in the literature some reported mathematical (empirical) expressions for such

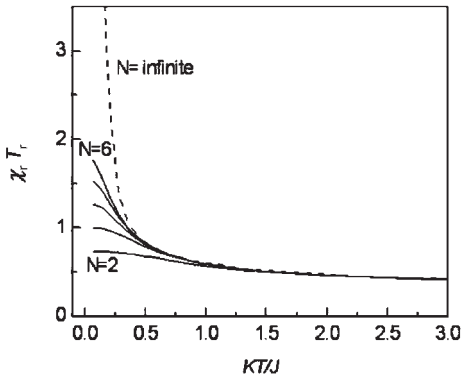

Figure 5. Theoretical curves of $\chi_r T_r$ versus kT/J.

chains but only in the case of AF coupling.[13] These formulas are not possible to apply for ferromagnetic complex **1**. To fit the magnetic data, we developed a new rational expression that can reproduce a ferromagnetic behavior of a $(AB)_N$ system, where $S_A = 1/2$ and $S_B = 1$. The Hamiltonian for the Heisenberg ferromagnetic chain with an alternate spin $S_i = 1/2$ and $S_{i+1} = 1$ can be written as:

$$H = -J\sum_{i=1}^{n} S_i S_{i+1}$$

where n is the number of spin pairs and J is ferromagnetic exchange interactions of the nearest neighbors; positive J means ferromagnetic coupling.

By applying the usual computational technique, based on the calculation of the properties of finite rings of increasing size ($N = 2-6$) and then extrapolating them to infinity, we determined the product of the reduced susceptibility and reduced temperature ($\chi_r T_r$) (see below) of ferromagnetic chains with an alternate spin $S_1 = 1/2$ and $S_2 = 1$. The calculations were computed with the CLUMAG program, which uses the irreducible tensor operator formalism (ITO).[14] Figure 5 shows the $\chi_r T_r$ curves of the chains when $N = 2-6$ (solid line) and the infinite curve calculated by extrapolation (dashed line).

An expression of the product $\chi_r T_r$ which depends on T_r can be generated easily by applying the same strategy reported in the literature[15] and fitting the theoretical $\chi_r T_r$ curve (N = infinite) to the following rational expression:

$$\chi_r T_r = (AT_r^2 + BT_r + C)/(DT_r^2 + ET_r + F)$$

where $\chi_r = \chi_M J/(11/4)Ng^2\beta^2$. We assumed that the local g factors were identical $g_{Cu} = g_{Ni} = g$, and the reduced temperature T_r is given by kT/J.

The $A-F$ coefficients calculated values through the infinite extrapolation are $A = 0.2916$, $B = 0.17654$, $C = -0.0192$, $D = 0.87479$, $E = -0.13315$, and $F = 0.00423$. The expression of the product $\chi_r T_r$ can be converted to product $\chi_M T$ in the habitual form to give:

$$\chi_M T = (11/4)(Ng^2\beta^2/k)[(A + BX + CX^2)/(D + EX + FX^2)]$$

where $X = J/kT = 1/T_r$. The expression is valid for $T_r = kT/J \geq 0.2$.

(13) (a) Drillon, M.; Gianduzzo, J. C.; Georges, R. *Phys. Lett.* **1983**, *96a*, 413. (b) van Koningsbruggen, P. J.; Kahn, O.; Nakatani, K.; Pei, Y.; Renard, J. P.; Drillon, M.; Legoll, P. *Inorg. Chem.* **1990**, *29*, 3325.

(14) Gatteschi, D.; Pardi, L. *Gazz. Chim. Ital.* **1993**, *123*, 231.

(15) Hall, J. W.; March, W. E.; Welles, R. R.; Hatfield, W. E. *Inorg. Chem.* **1981**, *20*, 1033.

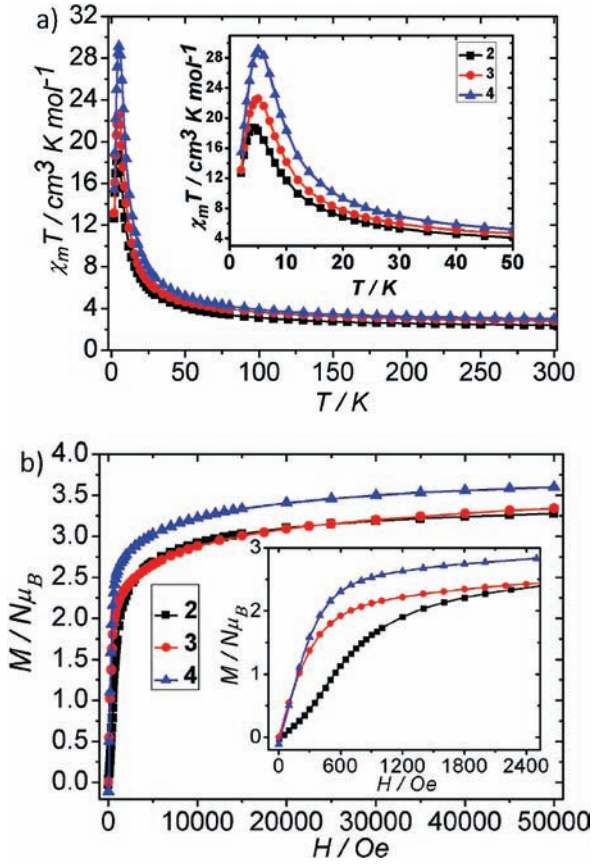

Figure 6. (a) Plots of observed $\chi_m T$ vs T at 0.2 T of **2**, **3**, and **4**. Inset: The $_mT$ vs T at 0.2 T of **2**, **3** and **4** at 2−50 K. (b) The field-dependent magnetizations plots ($M/N\mu_\beta$ vs H) at 2 K of **2**−**4**. Inset: The $M/N\mu_B$ vs H plots of **2**, **3**, and **4** at 2 K in the low-field zone (0−2500 Oe).

For the 1D chain in **1** was connected by the isonicotinate, and the expression of the χ_m can be converted to $\chi_m = \frac{\chi_M}{1-(zj'/Ng^2\beta^2)\chi_M}$ with the mean-field approximation[16] for interchain coupling zJ'.

The experimental data of **1** were fitted with the above equation in the range of 300−20 K. With allowance for variations in all the parameters, the best least-squares fit shown in Figure 3 gives $J = 49.98 \pm 0.94$ cm^{-1}, $zJ' = -1.14 \pm 0.04$ cm^{-1}, $g = 2.159 \pm 0.005$, and $R = 4.37 \times 10^{-4}$ (see also Figure S5, Supporting Information). The assumption of equal g-values for Cu^{II} and Ni^{II} is an approximation, for $g_{Ni} > g_{Cu}$. This is a justified approximation, since it should not greatly affect the calculated value of J (the parameter of interest). The positive value of J and the little negative value of the zJ' is consistent with the metamagnetic character of **1**.

The $\chi_m T$ vs T plot (χ_m is the molar magnetic susceptibility for one M^{II}−Cu^{II} couple) and the field-dependent magnetizations ($M/N\mu_B$ vs H) of **2**−**4** are shown in Figure 6. The part substitution of the Ni^{II} ions by the Co^{II} ions influences the magnetism of the complexes especially at low temperature. Like in **1** at room temperature, the $\chi_m T$ values of **2**−**4** smoothly increase up to 50 K and below 50 K increases quickly to a maximum ca. 19, 23, and 30 cm^3 mol^{-1}K for **2**−**4**, respectively, at 5 K. Above the maximum, the $\chi_m T$ curves decrease with further cooling. The values of the best-fit parameters from the magnetic data of **2**−**4** in the temperature range of 100−300 K through the Curie−Weiss law (Figure S3, Supporting Information) are: $\theta = 32.43$ K and $C = 2.14$ cm^3 K mol^{-1} for **2**, $\theta = 32.24$ K and $C = 2.56$ cm^3 K mol^{-1} for **3**, and $\theta = 31.74$ K and $C = 2.70$ cm^3 K mol^{-1} for **4**. This indicates the dominant feature of the magnetism of **2**−**4** is the ferromagnetic interactions in the 1D chain, as that in **1**. The field-dependent magnetizations at 2 K (Figure 6b) clearly corroborate the ferromagnetic coupling, and $M/N\mu_B$ values at 5 T are 3.27, 3.34, and 3.60 $N\mu_B$ for **2**−**4**, respectively, that approach to the saturation value. However in the low-field region the curve of complex **2** has a weak inflection like that in **1**, indicating that some metamagnetism also exists in **2**. From the first derivative of the $M/N\mu_B$ in the 0−2500 Oe (Figure S6, Supporting Information) a maximum at ca. 400 Oe is shown. Strong in-phase signals χ_m' with peaks at 2.6 K are shown in the ac measurements of complex **2**. The in-phase signals of **2** are frequency independent (Figure 7a). While weak out of in-phase signals χ_m'' of **2** were observed with small peaks and were frequency dependent. This suggested complex **2** is a metamagnet with small glass behaviors.

By contrasting the critical field of the metamagnetism in **1** and **2** as well as the tendency of the $M/N\mu_B$ vs H curves of **2**−**4**, it is clear to see that the metamagnetism was vanishing with the increase of the contents of Co^{II} ions. The trend of the weak inflection in the curve in **1** is disappeared in **3** and **4**, indicating the inexistence of the metamagnetic behavior. The ZFC and FC magnetization of **3** measured at 50 Oe is totally coincident that it excludes the ferromagnetic phase transition above 2 K (Figure S7, Supporting Information). However, the strong in and out-of-phase signals are detected in the ac susceptibility measurements of **3** and **4** at 10, 100, and 997 Hz in an oscillating field 3.5 Oe (Figure 7b,c). The in-phase χ_m' have peaks near 2.5 K, and the out-of-phase χ_m'' is frequency dependant but not reaching a maximum. This indicates the 3D antiferromagnetic order in **1** and **2** is destroyed in **3** and **4** due to increasing of the contents of Co^{II} ions. And **3** and **4** are more like a glass state or a superparamagnetism phase with very low block temperature.[17,18]

Similar to the complexes **1**−**4**, the $\chi_m T$ values (4.40 cm^3 mol^{-1} K at 300 K) of **5** increase from room temperature to a maximum and then drop but are field dependent from 25 to 2 K. At a field of 0.1 T they increase to ca. 100 cm^3 mol^{-1} K at 5 K but to 20 cm^3 mol^{-1} at a field of 10 000 Oe (Figure 8). This feature is characteristic of strong intrachain ferromagnetic coupling with weak interchain antiferromagnetic interactions. The values of the best-fit parameters from the magnetic data of **5** in the temperature 100−300 K through the Curie−Weiss law (Figure S3, Supporting Information) are: $\theta = 30.70$ K and $C = 4.04$ cm^3

(16) (a) Myers, B. E.; Berger, L.; Friedberg, S. A. *J. Appl. Phys.* **1969**, *40*, 1149. (b) O'Conner, C. J. *Prog. Inorg. Chem.* **1982**, *29*, 203.

(17) Mydosh, J. A. *Spin Glasses: An Experimental Introduction*; Taylor & Francis: London, 1993.

(18) (a) Mishra, A.; Pushkar, Y.; Yano, J.; Yachandra, V. K.; Wernsdorfer, W.; Abboud, K. A.; Christou, G. *Inorg. Chem.* **2008**, *47*, 1940. (b) Ma, Y.-S.; Li, Y.-Z.; Song, Y.; Zheng, L.-M. *Inorg. Chem.* **2008**, *47*, 4536. (c) Steiner, A.; Vittal, J. J.; Houri, A.; Clérac, R. *Inorg. Chem.* **2008**, *47*, 4918. (d) Huang, Y.-G.; Wang, X.-T.; Jiang, F.-L.; Gao, S.; Wu, M.-Y.; Gao, Q.; Wei, W.; Hong, M.-C. *Chem.—Eur. J.* **2008**, *14*, 10340. (e) Zheng, Y.-Z.; Lan, Y.-H.; Anson, E. C.; Powell, A. K. *Inorg. Chem.* **2008**, *47*, 10813.

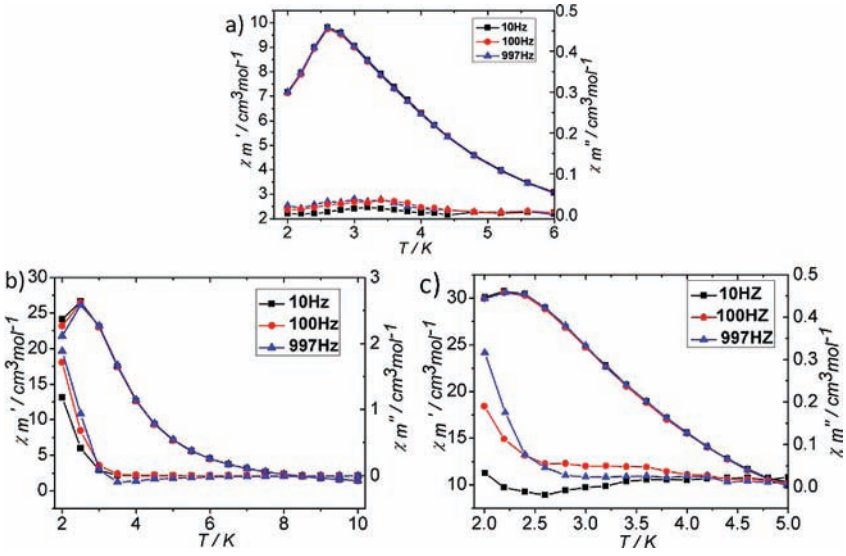

Figure 7. The ac plots for complex **2**−**4** with an oscillating field of 3.5 Oe: (a) for **2**, (b) for **3**, and (d) for **4**.

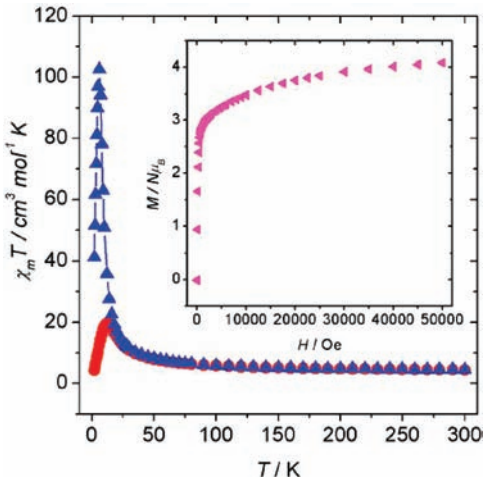

Figure 8. Plot of the $\chi_m T$ vs T for complex **5** (triangles 0.1 T Oe, and circles 1 T). Inset: The field-dependent magnetizations plots ($M/N\mu_B$ vs H) at 2 K for **5**.

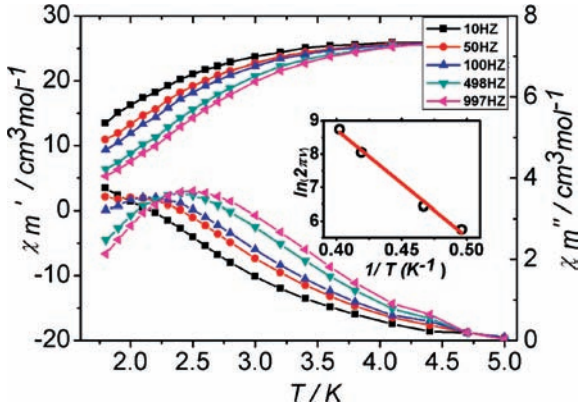

Figure 9. Temperature dependence of the real (top) and the imaginary (bottom) components of the ac susceptibility in a zero applied static field with an oscillating field of 2.5 Oe at a frequency of 10−997 Hz of **5**. The lines are guides. Inset: The Arrhenius plot obtained for the minor maximum in χ_m'' of the molar ac magnetic susceptibility of **5**.

K mol^{-1}. The C value is in the order expected for one Cu^{II} and one Co^{II} ion taking into account the spin−orbit coupling of the ground state in the Co^{II} ions. The field dependence of $\chi_m T$ is due either to the strong ferromagnetic coupling or, most likely, to the presence of ferromagnetic ordering at very low temperatures. The field-dependent magnetizations at 2 K are shown in Figure 8 inset: the $M/N\mu_B$ value at 5 T is close to 4 $N\mu_B$. The theoretical values for isolated Co^{II} ions are 2−2.5 $N\mu_B$ per Co atom.[19] By adding the contribution of the Cu^{II} ion, the expected value is, therefore, close to 4 $N\mu_B$. On the other hand, this plot does not follow at all the Brillouin function: at a low field there is a quasivertical increase from 0 to 3 $N\mu_B$. This feature corroborates both the strong ferromagnetic coupling and the probable magnetic ordering.

To further investigate the possible phase transition in **5** suggested by the field dependence of the $\chi_m T$ vs T curve and the magnetization at 2 K, the ZFC and FC magnetizations were measured from 11 down to 2 K under an applied field of 50 Oe. The plot of the ZFC/FC (Figure S8, Supporting Information) shows that close to 5 K there is a divergence of the two curves, which is the signature of the magnetic ordering. Anyway, this divergence is very small.

Ac dynamic susceptibility measurements of **5** were performed under an oscillating 2.5 Oe applied field in the 10−997 Hz interval. Both, the in-phase (χ_m') and out-of-phase (χ_m'') signals, define a peak at low temperatures confirming the occurrence of magnetic ordering and clear frequency dependence (Figure 9). Below 4.5 K, the real part χ_m' exhibits a maximum and then decreases on further cooling. In an ac field oscillating at a frequency of 10 Hz, the first step lies in the 4.5−3.0 K temperature range, where χ_m' diminishes smoothly and reaches an inflection point at T_i = 3.0 K. Below 3 K, the in-phase component cancels out very rapidly, in parallel with the abrupt decrease observed in the ZFC magnetization measurement. Below 4.5 K, χ_m'' increases steadily to reach a maximum and then vanishes. Both χ_m' and χ_m'' shift toward higher temperatures as the frequency becomes higher; χ_m'' defines a maximum between 1.9 and 2.5 K (50 and 997 Hz),

(19) Rueff, J.-M.; Masciocchi, N.; Rabu, P.; Sironi, A.; Skoulios, A. *Chem.—Eur. J.* **2002**, *8*, 1813 and references therein.

respectively. These features may indicate the presence of slow-relaxation effects, which are typical of SCM, or glass behavior. The presence of glassiness was discarded in view of the estimated frequency shift parameter, $\Phi = \Delta T_p/[T_p\Delta(\log f)] = 0.11$, which is in excellent agreement with that expected for superparamagnetic behavior.[17,20] The relaxation time was obtained from the Arrhenius law $\tau(T) = \tau_0\exp(-\Delta/k_BT)$, and the best set of parameters are $\tau_0 = 4.34 \times 10^{-10}$ s and $\Delta/k_B = 32.02$ K (Figure 8 insert), suggesting a thermally activated mechanism. These values are physically meaningful and in the range of the previously reported values for SMM and SCM systems.[2c,21] We tried to measure the Cole−Cole plots for the powder sample at different temperatures 2.0, 2.6, 2.8, 3.0, 3.5, 4, and 4.5 K (Figure S9, Supporting Information). Only that at 2 K shows an irregular semicircle, and it cannot be fitted with the Debye model to a reasonable α value, indicating a very large distribution of the relaxation time. The hysteresis loop at 2 K does not show any noticeable feature (Figure S10, Supporting Information). At 0 Oe there is a clear vertical zone from −3 to +3 $N\mu_B$, but all points are coincident when increasing or decreasing the field. The hysteresis loop, if it exists, should occur at temperatures lower than 2 K.

The three complexes are, actually, 3D $Cu^{II}-M^{II}$ networks. However, from the magnetic point of view, it may be considered as formed by 1D entities, in which Cu^{II} and M^{II} are alternated by $\mu_{1,1}$-N_3 and μ_2-carboxylate. The first bridge (azido end-on) creates ferromagnetic coupling and the second one (carboxylate *syn,syn*) provides antiferromagnetic coupling. The cooperated effects lead to strong ferromagnetic coupling between the Cu^{II} and M^{II} ions in the chains. The coupling transferred by the isonicotinate ligand is weakly antiferromagnetic. From **1**−**5**, as the Ni^{II} ions in the structure were replaced gradually by the Co^{II} ions with more single-ion anisotropy, the magnetic behaviors alter from 3D antiferromagnetic order to SCM-like. Usually the Co^{II} ions show Ising anisotropy when in a compressed octahedral geometry.[7b,22] In **2**−**5**, the M^{II} ions are in a slightly compressed distortion coordinated geometry. The tendency is toward Ising-like anisotropy as the increase of the content of Co^{II} ions was observed in the semilog plots of χ_mT vs $1/T$ of **1**−**5** (Figure S11a, Supporting Information). The linear behavior exhibited by the $\ln(\chi_mT)$ vs $1/T$ plot of **5** in the regime 5−15 K is indicative of the strong Ising-like anisotropy (giving a fitted of $\Delta_\xi/k_B = 23.27$ K, $C_{eff} = 4.66$ cm^3 K mol^{-1}, and $R = 0.999\%$ by the expression of $\chi_mT = C_{eff}\exp(\Delta_\xi/k_BT)$ (Figure S11b, Supporting Information).[23] In order to investigate the phase transition behavior of **5**, a noncritical-scaling method[24] was used. It is clear to see that in the $d\ln(T)/d\ln(\chi_mT)$ vs T curve of **5** (Figure S11c, Supporting Information) there is a linear regime, and a direct fit of the data from 10 to 30 K yields $T_C = 0$ K and $\gamma = \infty$. The value $T_C = 0$ K excludes the phase transition to long-range ordering above 0 K of this system, and $\gamma = \infty$ indicates the 1D Ising chain character of **5** that further confirms **5** is indeed a real 1D system.

Conclusion

The strategy for obtaining heterometallic azide complexes by assembling Cu^{II} and M ($M = Ni^{II}/Co^{II}$) azide and pyridyl carboxylate in hydrothermal condition allowed the synthesis of a new three-dimensional (3D) 3d−3d heterometallic azide complexe, $[CuNi_{1-x}Co_x(N_3)_2(isonic)_2]_\infty$ ($x = 0$ for **1**, $x = 0.3$ for **2**, $x = 0.5$ for **3**, $x = 0.6$ for **4** ,and $x = 1$ for **5**). The 3D structures can be described as EO azide and *syn,syn* carboxylates mixed bridged alternate Cu−M chains linked by the pyridyl groups. The magnetic properties are associated with metal ions in the chains. At low temperatures, **1** and **2** exhibit small metamagnetic behavior due to the weak antiferromagnetic coupling which is transferred by the isonicotinate ligands between chains. However as the Ni^{II} ions in the structure were replaced by the Co^{II} ions in **3**−**5**, the antiferromagnetic coupling between the azide bridged chains was diminished, and SCM-like behavior was present gradually. This observation conformed that the single-ion anisotropy might be the key for the magnetism of the SCM-like materials. Using the more anisotropy ions to replace the less one with similar coordinated geometry in the heterometallic system is feasible in constructing SCM- or SMM-like complexes.

Acknowledgment. We thank the financial support by the 973 Program of China (2007CB815305), the NSFC (20773068, 21031002), the Natural Science Fund of Tianjin, China (10JCZDJC22100), and the Spanish (CTQ2009-07264) and the Catalan (2005SGR-00593) governments.

Supporting Information Available: X-ray crystallographic data for complexes **1**−**5** in CIF format and Figures S1−S11. This material is available free of charge via the Internet at http://pubs.acs.org.

(20) Morrish, A. H. *The Physical Principles of Magnetism*; Wiley: New York, 1966.
(21) Sun, H.-L.; Wang, Z.-M.; Gao, S. *Coord. Chem.* **2010**, *254*, 1081 and references cited therein.
(22) Lescouzec, R.; Vaissermann, J.; Ruiz-Perez, C.; Lloret, F.; Carasco, R.; Julve, M.; Verdaguer, M.; Dromzee, Y.; Gatteschi, D.; Wernsdorfer, W. *Angew. Chem., Int. Ed.* **2003**, *42*, 1483.
(23) (a) Coulon, C.; Clérac, R.; Lecren, L.; Wernsdorfer, W.; Miyasaka, H. *Phys. Rev. B: Condens. Matter Mater. Phys.* **2004**, *69*, 132408. (b) Bogani, L.; Sessoli, R.; Pini, M. G.; Rettori, A.; Novak, M. A.; Rosa, P.; Massi, M.; Fedi, M. E.; Giuntini, L.; Caneschi, A.; Gatteschi, D. *Phys. Rev. B: Condens. Matter Mater. Phys.* **2005**, *72*, 064406.
(24) (a) Li, X.-J.; Wang, X.-Y.; Gao, S.; Cao, R. *Inorg. Chem.* **2006**, *45*, 1508. (b) Zhang, X.-M.; Hao, Z.-M.; Zhang, W.-X.; Chen, X.-M. *Angew. Chem., Int. Ed.* **2007**, *46*, 3456. (c) Hu, S.; Yun, L.; Zheng, Y.-Z.; Lan, Y.-H.; Powell, A. K.; Tong, M.-L. *Dalton Trans.* **2009**, 1897.